Research Article | Vol. 26, No. 2 | 22 Jan 2018 | OPTICS EXPRESS 1743
Optics EXPRESS

Multimode optical feedback dynamics in InAs/GaAs quantum dot lasers emitting exclusively on ground or excited states: transition from short- to long-delay regimes

HEMING HUANG,[1] LYU-CHIH LIN,[2] CHIH-YING CHEN,[2] DEJAN ARSENIJEVIĆ,[3] DIETER BIMBERG,[3,4] FAN-YI LIN,[2] AND FRÉDÉRIC GRILLOT[1,5,*]

[1]*LTCI, Télécom ParisTech, Université Paris-Saclay, 46 rue Barrault, 75013 Paris, France*
[2]*Institute of Photonics Technologies, Department of Electrical Engineering, National Tsing Hua University, Hsinchu 300, Taiwan*
[3]*Institut für Festkörperphysik, Technische Universität Berlin, Berlin 10623, Germany*
[4]*King Abdulaziz University, Jeddah 21589, Saudi Arabia*
[5]*Center for High Technology Materials, University of New-Mexico, 1313 Goddard SE, Albuquerque, NM, USA*
[*]*frederic.grillot@telecom-paristech.fr*

Abstract: The optical feedback dynamics of two multimode InAs/GaAs quantum dot lasers emitting exclusively on sole ground or excited lasing states is investigated. The transition from long- to short-delay regimes is analyzed, while the boundaries associated to the birth of periodic and chaotic oscillations are unveiled to be a function of the external cavity length. The results show that depending on the initial lasing state, different routes to chaos are observed. These results are of importance for the development of isolator-free transmitters in short-reach networks.

OCIS codes: (140.5960) Semiconductor lasers; (250.0250) Optoelectronics; (190.3100) Instabilities and chaos.

References and links

1. C. F. Lam, H. Liu, and R. Urata, "What devices do data centers need?" in Optical Fiber Communications Conference and Exhibition (OFC) of 2014 OSA Technical Digest Series (Optical Society of America, 2014), paper M2K.5.
2. Cisco white paper, "The Zettabyte Era: Trends and Analysis" (Cisco, 2016).
3. D. Bimberg, "Quantum dot based nanophotonics and nanoelectronics," Electron. Lett. **44**, 390 (2008).
4. G. Eisenstein and D. Bimberg, eds., *Green Photonics and Electronics* (Springer, 2017).
5. M. T. Crowley, N. A. Naderi, H. Su, F. Grillot, and L. F. Lester, "GaAs-Based Quantum Dot Lasers," in *Advances in Semiconductor Lasers*, J. J. Coleman, A. Bryce, and C. Jagadish, eds. (Academic Press, 2012), pp. 371–417
6. M. Grundmann, ed., *Nano-Optoelectronics*, NanoScience and Technology (Springer, 2002).
7. K. Nishi, K. Takemasa, M. Sugawara, and Y. Arakawa, "Development of quantum dot lasers for data-com and silicon photonics applications," IEEE J. Sel. Topics Quantum Electron. **23**, 1–7 (2017).
8. A. Y. Liu, S. Srinivasan, J. Norman, A. C. Gossard, and J. E. Bowers, "Quantum dot lasers for silicon photonics," Photonics Res. **3**, B1 (2015).
9. S. Chen, W. Li, J. Wu, Q. Jiang, M. Tang, S. Shutts, S. N. Elliott, A. Sobiesierski, A. J. Seeds, I. Ross, P. M. Smowton, and H. Liu, "Electrically pumped continuous-wave III-V quantum dot lasers on silicon," Nat. Photonics **10**, 307–311 (2016).
10. Ranovus Inc., "Ranovus announces availability of world's first quantum dot multi-wavelength laser and silicon photonics platform technologies to create a new cost and power consumption paradigm for DCI market," (Ranovus, 2016), http://ranovus.com/worlds-first-quantum-dot-multi-wavelength-laser-and-silicon-photonics-platform-technologies-for-dci-market/.
11. Y. Urino, N. Hatori, K. Mizutani, T. Usuki, J. Fujikata, K. Yamada, T. Horikawa, T. Nakamura, and Y. Arakawa, "First demonstration of athermal silicon optical interposers with quantum dot lasers operating up to 125 °C," J. Lightw. Technol. **33**, 1223–1229 (2015).
12. N. Zhuo, J.-C. Zhang, F.-J. Wang, Y.-H. Liu, S.-Q. Zhai, Y. Zhao, D.-B. Wang, Z.-W. Jia, Y.-H. Zhou, L.-J. Wang, J.-Q. Liu, S.-M. Liu, F.-Q. Liu, Z.-G.Wang, J. B. Khurgin, and G. Sun, "Room temperature continuous wave quantum dot cascade laser emitting at 7.2 μm," Opt. Express **25**, 13807–13815 (2017).

#318053 https://doi.org/10.1364/OE.26.001743
Journal © 2018 Received 19 Dec 2017; accepted 8 Jan 2018; published 16 Jan 2018

Optics EXPRESS

13. A. Spott, E. J. Stanton, N. Volet, J. D. Peters, J. R. Meyer, and J. E. Bowers, "Heterogeneous integration for mid-infrared silicon photonics," IEEE J. Sel. Top. Quantum Electron. **23**, 1–10 (2017).
14. D. O'Brien, S. Hegarty, G. Huyet, J. McInerney, T. Kettler, M. Laemmlin, D. Bimberg, V. Ustinov, A. Zhukov, S. Mikhrin, and A. Kovsh, "Feedback sensitivity of 1.3 μm InAs/GaAs quantum dot lasers," Electron. Lett. **39**, 1819 (2003).
15. K. Mizutani, K. Yashiki, M. Kurihara, Y. Suzuki, Y. Hagihara, N. Hatori, T. Shimizu, Y. Urino, T. Nakamura, K. Kurata, and Y. Arakawa, "Optical I/O core transmitter with high tolerance to optical feedback using quantum dot laser," in 2015 European Conference on Optical Communication (ECOC) (2015), paper 0263.
16. D. Arsenijević and D. Bimberg, "Quantum-dot lasers for 35 gbit/s pulse-amplitude modulation and 160 gbit/s differential quadrature phase-shift keying," Proc. SPIE **9892**, 9892 (2016).
17. C. Wang, B. Lingnau, K. Lüdge, J. Even, and F. Grillot, "Enhanced dynamic performance of quantum dot semiconductor lasers operating on the excited state," IEEE J. Quantum Electron. **50**, 723–731 (2014).
18. Z.-R. Lv, H.-M. Ji, X.-G. Yang, S. Luo, F. Gao, F. Xu, and T. Yang, "Large Signal Modulation Characteristics in the Transition regime for two-state lasing quantum dot lasers," Chinese Phys. Lett. **33**, 124204 (2016).
19. B. J. Stevens, D. T. D. Childs, H. Shahid, and R. A. Hogg, "Direct modulation of excited state quantum dot lasers," Appl. Phys. Lett. **95**, 061101 (2009).
20. D. Arsenijević, A. Schliwa, H. Schmeckebier, M. Stubenrauch, M. Spiegelberg, D. Bimberg, V. Mikhelashvili, and G. Eisenstein, "Comparison of dynamic properties of ground- and excited-state emission in p-doped InAs/GaAs quantum-dot lasers," Appl. Phys. Lett. **104**, 181101 (2014).
21. F. Grillot, B. Dagens, J.-G. Provost, H. Su, and L. F. Lester, "Gain compression and above-threshold linewidth enhancement factor in 1.3-μm InAs-GaAs quantum-Dot lasers," IEEE J. Quantum Electron. **44**, 946–951 (2008).
22. F. Zubov, M. Maximov, E. Moiseev, A. Savelyev, Y. Shernyakov, D. Livshits, N. Kryzhanovskaya, and A. Zhukov, "Observation of zero linewidth enhancement factor at excited state band in quantum dot laser," Electron. Lett. **51**, 1686–1688 (2015).
23. C. Mesaritakis, C. Simos, H. Simos, S. Mikroulis, I. Krestnikov, E. Roditi, and D. Syvridis, "Effect of optical feedback to the ground and excited state emission of a passively mode locked quantum dot laser," Appl. Phys. Lett. **97**, 061114 (2010).
24. A. Röhm, B. Lingnau, and K. Lüdge, "Ground-state modulation-enhancement by two-state lasing in quantum-dot laser devices," Appl. Phys. Lett. **106**, 1–6 (2015).
25. F. Grillot, N. A. Naderi, J. B. Wright, R. Raghunathan, M. T. Crowley and L. F. Lester, "A dual-mode quantum dot laser operating in the excited state," Appl. Phys. Lett. **99**, 1110–1113 (2011).
26. J. D. Walker, D. M. Kuchta, and J. S. Smith, "Wafer-scale uniformity of vertical-cavity lasers grown by modified phase-locked epitaxy technique," Electron. Lett. **29**, 239-240 (1993).
27. H. Huang, D. Arsenijević, K. Schires, T. Sadeev, D. Bimberg, and F. Grillot, "Multimode optical feedback dynamics of InAs/GaAs quantum-dot lasers emitting on different lasing states," AIP Adv. **6**, 125114 (2016).
28. A. Kovsh, N. Maleev, A. Zhukov, S. Mikhrin, A. Vasil'ev, E. Semenova, Y. Shernyakov, M. Maximov, D. Livshits, V. Ustinov, N. Ledentsov, D. Bimberg, and Z. Alferov, "InAs/InGaAs/GaAs quantum dot lasers of 1.3 μm range with enhanced optical gain," J. Cryst. Growth **251**, 729–736 (2003).
29. O. Stier, M. Grundmann, and D. Bimberg, "Electronic and optical properties of strained quantum dots modeled by 8-band k·p theory," Phys. Rev. B **59**, 5688 (1999).
30. A. Schliwa, M. Winkelnkemper, and D. Bimberg, "Few-particle energies versus geometry and composition of $In_xGa_{1x}As/GaAs$ self-organized quantum dots," Phys. Rev. B **79**, 075443 (2009).
31. N. Schunk and K. Petermann, "Stability analysis for laser diodes with short external cavities," IEEE Photon. Technol. Lett. **1**, 49–51 (1989).
32. J. Ohtsubo, *Semiconductor Lasers: Stability, Instability and Chaos*, Springer Series in Optical Sciences (Springer, 2010).
33. J. P. Toomey, D. M. Kane, C. McMahon, A. Argyris, and D. Syvridis, "Integrated semiconductor laser with optical feedback: transition from short to long cavity regime," Opt. Express **23**, 18754 (2015).
34. N. Gavra and M. Rosenbluh, "Behavior of the relaxation oscillation frequency in vertical cavity surface-emitting laser with external feedback," J. Opt. Soc. Am. B **27**, 2482–2487 (2010).
35. M. Stubenrauch, G. Stracke, D. Arsenijević, A. Strittmatter, and D. Bimberg, "15 Gb/s index-coupled distributed feedback lasers based on 1.3 μm InGaAs quantum dots," Appl. Phys. Lett. **105**, 011103 (2014).

1. Introduction

The transfer of massive amounts of information is no longer limited to optical long-distance transoceanic links or backbone networks. Today data through-put in shorter reach networks is larger. Metropolitan and access networks and finally fiber-to-the-home systems show huge growth rates. In data centers and supercomputers most amounts of information are exchanged between servers. Intra-chip and inter-chip interconnects are coming next [1,2]. New requirements in particular of the energy consumption showing trade-offs with data rates must be now carefully

Optics EXPRESS

considered in the design and operation of new generations of photonic devices [3, 4]. Owing to their truly discrete energy states, InAs/GaAs quantum dot (QD) lasers offer superior continuous-wave properties as compared to their quantum well (QW) counterparts [3–7]. The lower threshold current and the higher temperature stability make QD lasers much better candidates for reducing the power consumption [3] being vital for silicon photonic integration [8–11]. Let us stress that recent works have also reported the possibility to extend the heterogeneous silicon platforms to the mid-infrared window hence paving the way of novel types of sensor applications [12, 13].

Commonly, QD lasers are engineered to operate on the ground-state (GS) transition because of its lower threshold current density. Owing to the strong damping of the relaxation oscillations, GS lasing emission commonly exhibits a higher resistance to external optical feedback which is desired for laser stability and isolator-free applications [14, 15]. However, it is known that this strong damping of GS QD laser limits their modulation capabilities at room temperature [16–20]. In order to increase the speed, prior studies have proposed to take advantage of the stimulated emission originating from the first excited state (ES) transition [18–20]. Owing to a faster carrier capture as well as twice larger higher saturated gain, ES QD lasers are more promising for high-speed applications. For instance, the twice larger degeneracy of the ES translates into a larger maximum gain and differential gain and smaller nonlinear gain compression. For instance, it was shown that ES lasers exhibit a much smaller K-factor as compared to GS ones which is of first importance for maximizing the possible bandwidth of high-speed transmitters [16]. The first experimental demonstration performed at the link level was achieved with 1.3 μm InAs/GaAs QD lasers emitting on the first ES transition, for which modulation capabilities up to 25 Gbps (OOK) and 35 Gbps (PAM) have been successfully reported [16, 20]. In addition, it was shown that ES QD lasers can exhibit a near-zero linewidth enhancement factor (LEF), which is crucial for a multitude of applications [21, 22].

This work reports on comparative experiments dealing with the multimode optical feedback dynamics [14] of two InAs/GaAs QD Fabry-Perot (FP) lasers having identical active regions but emitting from different energy states. The present QD lasers do not exhibit a two-state lasing dynamics where ES and GS lasing can take place simultaneously [23, 24], but instead they emit either exclusively on the GS or the ES. In practice, the ES emission can be selected by multiple ways, e.g. by shortening the cavity length, using proper facet coatings, or directly through a dichroic mirror [17, 20]. An alternative approach presents a DFB laser, for which the grating pitch is adjusted to the ES transition [25]. Here, the ES selection is simply obtained by exploiting the natural wavelength dispersion of the photoluminescence (PL) peak across the entire wafer [26]. The fabrication yield is relatively high, and the wafer uniformity is very good with variations between material parameters of the order of 1%. In order to avoid problems which might arise from some GS-ES interplay dynamics, for this work independent devices for ES and GS emission were processed, rather than a single section device emitting on both energy states [23, 25]. As opposed to our previous studies [27], which were concentrated only on long-delay feedback, this paper goes an important step beyond by analyzing the full transition from short- to long-delay regimes. Boundaries associated to the birth of both periodic and chaotic oscillations are unveiled and are shown to depend on the external cavity length. The experiments show richer feedback dynamics in the ES QD laser as compared to GS lasers in which no chaotic pulsations are observed. The present study brings now a detailed understanding of the nonlinear dynamics of multimode QD lasers and is of paramount importance for the development of feedback resistant transmitters.

2. Experimental configuration

The active region of both devices, one emitting solely on GS and the other solely on ES, is based on a dot-in-well structure, including 10 InAs dot sheets grown by molecular beam epitaxy (MBE),

Optics EXPRESS

and embedded in InGaAs quantum wells [28]. The dot lateral extension is around 30 nm, with a dot density of 3 ~ 5×10^{10} cm^{-2}. Lasers are left as-cleaved and cavity lengths are both 1 mm long while the ridge waveguide etched through the active region is 2 μm wide [28]. Figure 1 displays the LIs curves of both lasers. For the GS laser, the threshold current I_{th} is of 16.5 mA, the external efficiency is 21%, and the gain peak wavelength is ~1300 nm. For the ES one, the threshold current I_{th} is of 88.5 mA, the external efficiency is 11%, and the gain peaks is at ~1220 nm. The insets of Fig. 1 display the optical spectra taken at $1.75 \times I_{th}$, the insets (II) highlight the center of the emission marked by the red rectangle boxes in insets (I). Most interestingly the ES QD laser does exhibit a modulated optical spectral envelope in contrast to the GS QD laser [27]. Qualitatively, these peculiar properties can be attributed to a competing number of allowed excitonic transitions from the ES state based both on the ES electron doublet splitting as well as on the variety of energetically close laying hole states [29, 30]. The experiments described hereinafter are performed at room temperature (298K). As shown in Fig. 1(b), to avoid power roll-over, the bias current was fixed at 160 mA (~ $1.75 \times I_{th}$) to maximize the ES QD laser output power. The same bias-to-threshold ratio was kept for the whole investigation of the GS laser dynamics. The operation points are indicated in Fig. 1 with black dots.

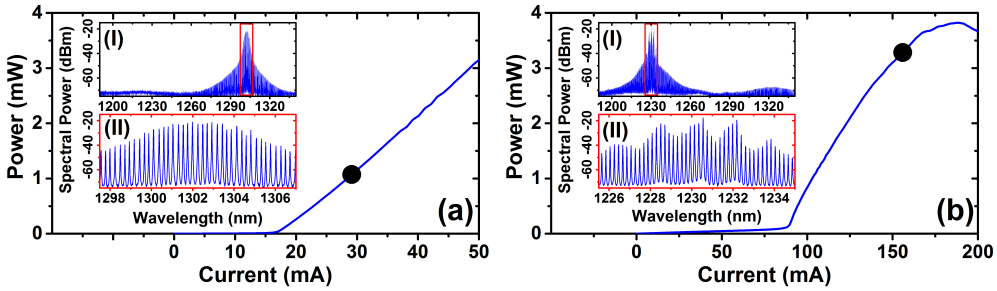

Fig. 1. L-I dependence of the (a) GS and (b) ES QD lasers. The insets (I) show the optical spectra taken at 1.75×I_{th} for both lasers while the insets (II) highlight the center of the emission marked by the red rectangle in insets (I). The black dots indicate the operating points of both lasers as discussed in the text.

Figure 2 depicts the free-space optical feedback setup. The QD lasers are mounted on a suspended optic table to minimize the environmental perturbations. The free-space external cavity is located on the left side of the laser, the lasing emission from the rear facet is coupled by an AR coated lens and reflected by a movable mirror which allows us to adjust the external cavity length L_{ext}. The latter is varied from 2 cm up to 50 cm, which corresponds to a ratio f_{RO}/f_{ext} ranging from 0.2 to 10 with f_{RO} the relaxation oscillation frequency of the solitary laser and $f_{ext} = c/2L_{ext}$ the frequency of the external cavity. Such a tuning allows continuously probing the laser dynamics both within short- and long-delay regimes corresponding to the cavity lengths where the ratio f_{RO}/f_{ext} is <1 or >1, respectively [31]. For each L_{ext}, the focus of the lens is readjusted in order to collimate safely the coupled light onto the mirror. The feedback strength r_{ext}, defined as the ratio of the returning power to the laser output power, is controlled by a free-space variable optical attenuator (VOA). The feedback strength r_{ext}, which takes into account the coupling loss between the facet and the external cavity is calculated with an accuracy better than 0.01%. Due to the different output beam divergence, the range of feedback strength r_{ext} is not exactly the same for both devices. For the GS laser, r_{ext} ranges from 0.04% to ~ 75%, while it ranges from 0.04% to ~ 55% for the ES one. Emission from the front facet is then coupled by an AR coated lens-end fiber and isolated for further analysis. On the detection path, an optical spectrum analyzer (OSA) and an electrical spectrum analyzer (ESA) are connected to monitor the dynamics simultaneously.

Optics EXPRESS

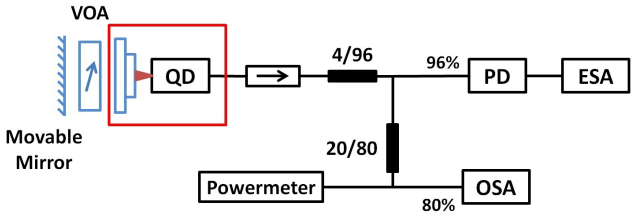

Fig. 2. Free-space optical feedback apparatus. PD: photo-diode; ESA: electrical spectrum analyzer; OSA: optical spectrum analyzer; VOA: variable optical attenuator.

3. Results and discussion

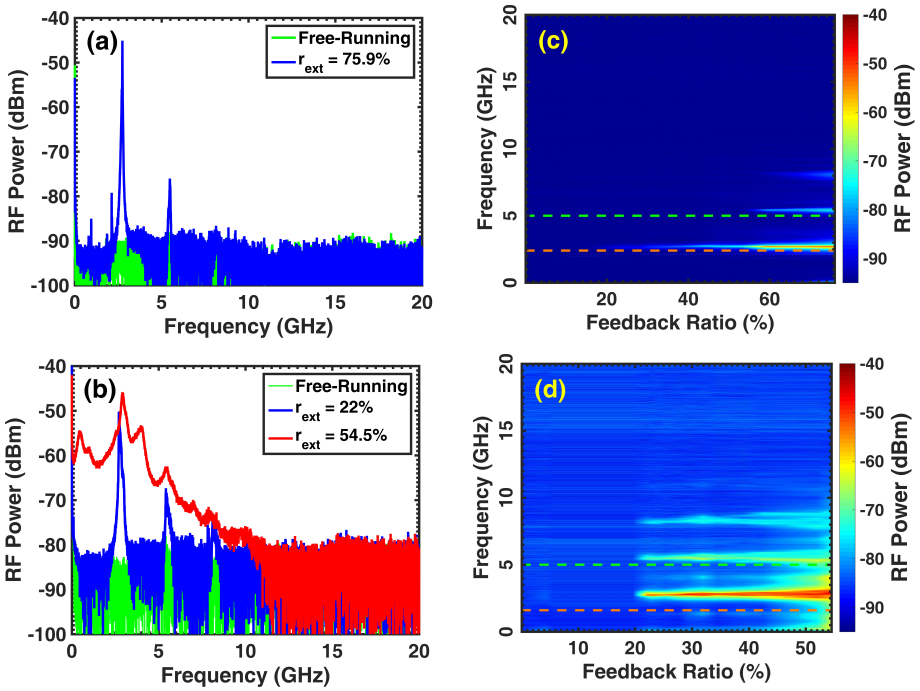

Fig. 3. RF spectra measured with L_{ext} = 3 cm (f_{ext}=5 GHz): (a) GS QD laser under free-running operation (black) and maximal feedback ratio of 75.9% (blue); (b) ES QD laser under free-running operation (black), 22% optical feedback (blue) and maximal feedback ratio of 54.5% (red). (c) and (d) RF spectral mappings as a function of the feedback ratio for the GS and ES QD lasers.

Figures 3(a) and 3(b) depict the radio-frequency (RF) spectra of both QD lasers operating under free-running conditions and short-delay feedback with L_{ext} = 3 cm (f_{ext}=5 GHz). Without feedback, the free-running RF spectra remain flat with a level of RF power comparable to that of the noise floor. In order to get a more complete overview of the dynamics, Figs. 3(c) and 3(d) also display the RF spectral mapping with respect to the feedback ratio, assuming the same experimental conditions. The color bar represents the RF power measured by the photo-detector. The green dashed lines correspond to the frequency of the external cavity (f_{ext} = 5 GHz) while the

Optics EXPRESS

orange ones indicate the level of the relaxation oscillation frequencies f_{RO} of the free-running lasers. Let us stress, that the relaxation oscillation frequencies f_{RO} are not directly extracted from the setup presented Fig. 2. Instead, in order to reduce the loss, the output of the laser was directly sent to the photodiode and the ESA allowing better accuracy of the measured values. At $1.75\times I_{th}$, f_{RO} of the GS QD laser is about 2.4 GHz, while the ES QD laser exhibits a smaller value of 1.6 GHz. The difference between these values can be attributed to larger thermal effects in the ES QD lasers driven at 5 times larger current, as shown in the Fig. 1(b). In addition, the inhomogeneous broadening due to much larger energy level dispersion (see inset II of Fig. 1(b)) must be taken into account as well. Overall, both lasers remain perfectly stable for low value of r_{ext} (a few percent), then Hopf bifurcation with the undamping of the relaxation oscillations through period one oscillations arise above ~ 40% for the GS laser and ~ 20% for the ES one. Under optical feedback, characteristic frequencies are observed which differ, depending on the nature of the lasing transition. For instance, Fig. 3(a) shows that for the largest feedback ratio (i.e. r_{ext}=75.9%), the GS QD laser is driven by periodic dynamics. In this regime, the dominant contribution peaking at about 2.5 GHz results from the relaxation oscillations, as seen in Fig. 3(c). Interestingly, this device emitting exclusively on the GS transition does not exhibit a clear route to chaos. Thus, the dynamics evolves from a stable solution to periodic oscillations without any chaotic pulsations, whatever the feedback level is. For the QD laser emitting on the ES transition, Fig. 3(b) unveils a more regular route to chaos with periodic oscillations (blue) at 2.5 GHz (r_{ext}=22%) followed by a chaotic regime (red) characterized by a high pedestal of noise level (r_{ext}=54.5%). It is true that the periodic oscillation frequency observed in ES laser here is similar to that of the GS laser, however, as the corresponding r_{ext} differs, the excited periodic oscillations do not behave the same way. As seen from Fig. 3(d), the dominant frequency slightly differs from the relaxation oscillation frequency of the ES laser, which can be attributed to the increase of the refractive index due to thermal effects at this higher bias level.

Although the two lasers are based on the same active medium, our results show non-symmetrical responses to optical perturbations. Indeed, because the stimulated emission of the first QD laser exclusively originates from the GS transition, the carrier dynamics involves transport, capture and relaxation, unlike for the ES. In other words, the ES QD laser alone exhibits richer optical feedback dynamics. The extra carrier transport required for emission on the GS leads to a larger damping rate γ_D preventing chaotic oscillations even at the highest feedback ratios. According to the data from our previous work, the damping factor γ_D of this ES QD laser was estimated to be much smaller of about 0.6 GHz, as compared to that of the GS QD one being above 18 GHz [27]. Besides, it has to be noted that the shapes of the optical spectra may also affect the sensitivity to optical feedback. As shown in the insets (II) of Fig. 1(a) and 1(b)), the ES QD laser suffers from a stronger modal competition as compared to the GS laser [27, 29, 30].

In what follows, the RF spectral mappings are now used to extract the boundaries associated with the periodic and chaotic states both in short- and long-delay regimes. To do so, the following criteria are used. First, a threshold of the periodic oscillation is defined as the excited peak being 5 dB above the free-running noise level. Second, the threshold of the chaotic oscillation is defined as the noise level of the RF spectrum being more than 10 dB above the free-running noise spectrum. Based on these two criteria, Fig. 4 depicts the boundaries extracted at $1.75\times I_{th}$ as a function of the external cavity length L_{ext}. The separation between the short- and long-delay regimes is marked by the vertical line (orange) corresponding to the condition $f_{RO}/f_{ext} = 1$. For improved precision, measurements are performed by varying the external cavity length every centimeter close to the transition while larger steps are taken above this area. Due to the absence of chaos in the GS QD laser, only boundaries associated to the transition between fixed points and periodic oscillations (blue) are reported in Fig. 4(a), while for the ES QD one those from periodic to chaotic oscillations (red) are present in Fig. 4(b). Because the GS QD laser is strongly overdamped, the lower limit of the periodic boundaries is always found at larger feedback

Optics EXPRESS

levels. In addition, within the short-delay regime ($f_{RO}/f_{ext} < 1$), boundaries show some residual undulations. This effect directly results from inferences between internal and external cavity modes [32], which means that the extrema correspond to situations where the laser is either stable or unstable. In long-delay regime ($f_{RO}/f_{ext} > 1$), the feedback ratio delimiting the boundaries keeps decreasing, until it progressively becomes rather independent of the external cavity length. Hence the feedback phase exhibits no undulations. This smooth transition arising between the short and long-delay regimes is different from what typically occurs for single-frequency lasers for which a sharper transition is usually observed [33].

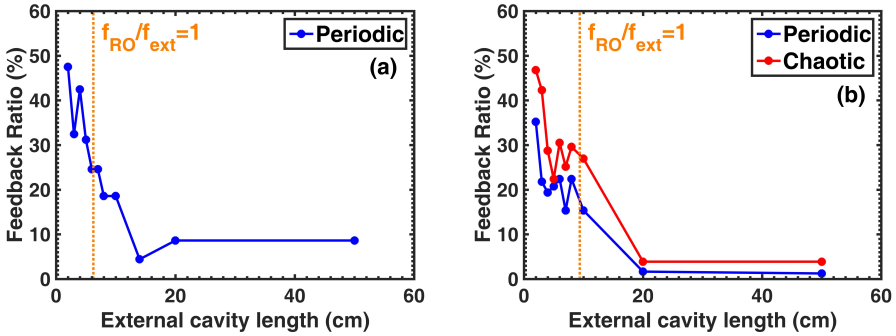

Fig. 4. Extracted boundaries of periodic (blue) and chaotic oscillations (red) with respect to the external cavity length L_{ext} measured at 1.75 $\times I_{th}$ for (a) GS and (b) ES QD lasers.

In order to further understand the impact of the optical feedback, our results are now described by a standard rate equation model. To do so, let A, ϕ, and N be the amplitude, the phase and the carrier density respectively such as [32]:

$$\begin{aligned}
\frac{dA}{dt} &= \frac{1}{2}\Gamma a\{[N(t)-N_t]-\frac{1}{\tau_p}\}A(t)+\kappa A(t-\tau_{ext})\cos\theta(t)\\
\frac{d\phi}{dt} &= \frac{1}{2}\alpha_H\Gamma a\{[N(t)-N_t]-\frac{1}{\tau_p}\}A(t)+\kappa\frac{A(t-\tau_{ext})}{A}\sin\theta(t)\\
\frac{dN}{dt} &= \frac{I}{qV}-\frac{N(t)}{\tau_c}-a[N(t)-N_t]A^2(t)
\end{aligned} \tag{1}$$

with $\tau_{ext} = f_{ext}^{-1}$ and $\theta(t) = \omega_0\,\tau_{ext} + \phi(t) - \phi(t-\tau_{ext})$ the respective round-trip time and feedback phase in the external cavity, Γ the confinement factor, a the linear gain coefficient, N_t the carrier density at transparency, τ_p the photon lifetime, α_H the LEF, I the pump current, q the electron charge, V the active region volume, and τ_c the carrier lifetime. The coefficient κ in the above equations is linked to the feedback ratio r_{ext} through the expression:

$$\kappa = \frac{1-R}{2\tau_{in}\sqrt{R}}\sqrt{r_{ext}} \tag{2}$$

with τ_{in} and R the internal photon round-trip time and the facet reflectivity subjected to the optical feedback. Assuming small perturbations of the steady-states A_s, ϕ_s and N_s such as $A_s + \delta A e^{\gamma t}$, $\phi_s + \delta\phi e^{\gamma t}$ and $N_s + \delta N e^{\gamma t}$, the Jacobian matrix can be extracted such as:

$$\mathcal{M} = \begin{pmatrix} -\kappa K\cos(\omega_s\tau_{ext}) & -\kappa K A_s\sin(\omega_s\tau_{ext}) & \frac{1}{2}\Gamma a A_s \\ \kappa\frac{K}{A_s}\sin(\omega_s\tau_{ext}) & -\kappa K\cos(\omega_s\tau_{ext}) & \frac{1}{2}\alpha_H\Gamma a \\ -2a(N_s-N_{tr})A_s & 0 & -(aA_s^2+\frac{1}{\tau_c}) \end{pmatrix} \tag{3}$$

Optics EXPRESS

The characteristic equation is then given by the determinant $D(\gamma)$ [32] as:

$$D(\gamma) = \gamma^3 + 2[\gamma_D + \kappa K\cos(\omega_s\tau_{ext})]\gamma^2 + [\kappa^2K^2 + 4\kappa K\cos(\omega_s\tau_{ext})\gamma_D + \omega_{RO}^2]\gamma + \{\kappa^2K^2\gamma_D + \omega_{RO}^2\kappa K[\cos(\omega_s\tau_{ext}) - \alpha_H\sin(\omega_s\tau_{ext})]\} = 0 \quad (4)$$

where $f_{RO} = \omega_{RO}/2\pi$ is the relaxation oscillation frequency of the free-running laser. Taking $\gamma = i2\pi f$ and assuming a weak feedback configuration (i.e. $(2\pi f_{RO})^2 \gg \kappa^2$), the excited periodic frequency associated to the stability boundaries is expressed as follows [32]:

$$f_p^2 - f_{RO}^2 = \frac{\gamma_D}{\pi} f_p \cot\left(\frac{\pi f_p}{f_{ext}}\right) \quad (5)$$

Equation (5) tells that under weak feedback, the excited periodic frequencies f_P oscillate from either side of the free-running relaxation oscillation frequency f_{RO} with respect to the external cavity length. It is possible to find some positions of the external cavity for which the laser stability is further enhanced.

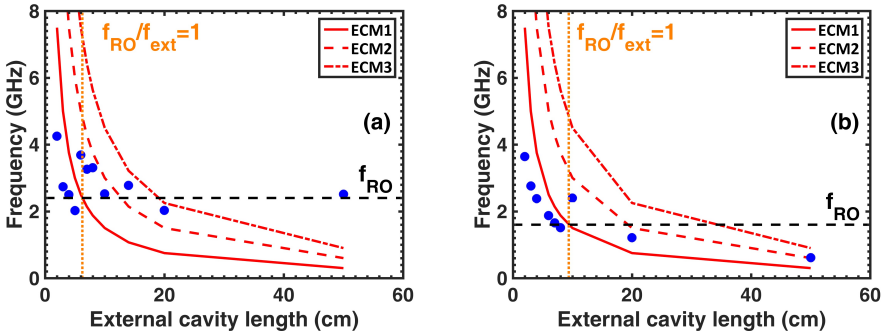

Fig. 5. Excited periodic frequency f_P at the stability boundary between fixed points to periodic oscillations with respect to the external cavity length L_{ext} measured at 1.75×I_{th} for (a) GS and (b) ES QD lasers.

Figure 5 shows the extracted f_P (blue points) associated to the stability boundary between fixed points and periodic oscillations for both QD lasers. As previously mentioned, in order to reach a better precision, each point is obtained by considering a fine tuning step of the external cavity length especially close to the transition. The vertical lines (orange) corresponding to $f_{RO}/f_{ext} = 1$ is once again indicating the separation of regimes. The lines in red give the frequency branches of the three first external cavity modes (ECM) with $f_n = n \times f_{ext}$ with n=1,2,3 respectively. In the short-delay regime and for some positions slightly above $f_{RO}/f_{ext} = 1$, the excited frequency continuously decreases with the external cavity length with some oscillations located on either side of f_{RO}. This effect is notably enhanced when the external frequencies are larger than the relaxation frequency, in qualitative agreement with Eq. (5) and with the evolution of the boundaries shown in Fig. 4. However, it turns out that the observed oscillations are not perfectly symmetric on both sides of f_{RO} whatever the lasing transition is. This discrepancy is attributed to the stronger feedback conditions (r_{ext} >2% and κ >6.4 GHz > f_{RO}) used in the experiments, hence the domain of validity of Eq. (5) is on verge. This experimental limitation, which is enhanced in the short cavity regime, is a result of the nature of the QD lasers, hence making the κ-factor always larger than the relaxation oscillation frequency. Interestingly, from Fig. 5, for some positions of the external cavity length, the maxima tend to coincide with the external cavity mode frequencies. In other words, when the maxima perfectly match with the external

Optics EXPRESS

branches, the relaxation oscillations are undamped because the damping factor is decreased as the length of the external cavity increases [34]. As such, it becomes more favorable for the system to switch to the next frequency branch with a higher damping. Then, when QD lasers enter into the long-delay regime, the sensitivity to the feedback phase is lost, and the excited frequency converges towards f_{RO}. However, the convergence is not perfect for the ES lasing transition, probably because of the very low damping rate observed in this laser. Lastly, with the increase of optical feedback at a fixed external cavity length, the laser oscillation evolves to a periodic state after crossing the boundary. However, when the external cavity length satisfies the condition $L_{ext} = mc/2\pi f_{RO}$, the laser can constructively couple with the external cavity, meaning that a larger fraction of feedback light is required to destabilize it. The stable area is relatively larger at this location, but the laser can become unstable after the feedback exceeds the critical point corresponding to the birth of chaotic oscillations (see Fig. 4).

4. Conclusion

This work provides fundamental insight on the multimode optical feedback dynamics of InAs/GaAs QD lasers emitting on different lasing states. Although the two lasers are made from the same active medium, their responses to the external perturbation are found not much alike. The GS laser displays a strong resistance to optical perturbations without any chaotic pulsations whatever the measured external cavity length and feedback strength. In contrast, the ES laser exhibits richer nonlinear dynamics with both periodic and chaotic oscillations. Such a difference is attributed to the very large damping factor of the GS laser preventing any chaotic oscillations even at the largest feedback ratios. Lastly, the evolution of the extracted boundaries and excited periodic frequency unveils a clear dependence on the external cavity length of oscillations in the short-delay regime, while in the long-delay regime the system becomes rather independent of the feedback phase. However, in this case, the transition from short- to long-delay regime is not as sharp as that is usually observed in single-mode lasers. As a conclusion, these results provide useful guidelines for featuring quantum dot laser based system solutions with low energy consumption, which is of prime importance for short reach networks. Since quantum dots are touted to be very promising for silicon photonics [9], this work provides important information for the realization of on-chip isolator-free active-components. For instance, a recent work has reported a 25 Gbps QD silicon transmitter operating without optical isolator [15]. Our future work will extend these investigations to single mode InAs/GaAs distributed feedback lasers [35]. Modeling taking into account the fundamental features of quantum dots as well as both single mode and multimode configurations will be performed.

Fundings

Campus France (PhC Orchid No. 33721SC); the Institut Mines Télécom (IMT) through the Futurs & Ruptures program; Ministry of Science and Technology (Taiwan) contracts MOST 105-2911-I-007-501 and 103-2112-M-007-019-MY3.